

# A Motion Compensation Approach for Dental Cone-beam Region-of-interest Imaging

Tao Sun, Johan Nuyts, Roger Fulton

**Abstract**— Motion of the patient affects image quality in dental cone-beam imaging. While efforts are always made to minimize motion during the scan, relatively little attention has been given to methods of compensating for the motion during the reconstruction of the image. In a previous study, we proposed an approach to iteratively estimate and compensate for rigid head motion within the reconstruction process for helical CT. This study reports on an extension of this method to mitigate the effect of the limited field-of-view (FOV) in the dental scan. The new method was evaluated with simulations. The quality of the reconstructed images was improved substantially after motion compensation. The proposed method eliminated most of the motion-induced artifacts in dental region-of-interest (ROI) imaging.

**Index Terms**—Cone-beam Computed Tomography (CT), dental imaging, motion estimation, motion compensation.

## I. INTRODUCTION

Patient motion is one of the main causes of visible image artifacts in dental imaging. Unlike clinical helical CT, dental imaging most commonly uses cone-beam CT, which requires a longer scan time and thus increases the probability of patient motion during the examination. The motion artifacts in the reconstructed image can degrade the image quality, adversely affecting diagnosis or treatment planning [1], [2]. Further problems arise when metal implants are present together with the movement [3].

Various efforts have been made to prevent patient motion using restraining devices. However, relatively little has been published on methods to reduce motion artifacts in the reconstructed images. Some approaches detect the motion by tracking artificial or anatomical landmarks in the image or projection domains [4], [5]. Others minimize an image-based cost-function which detects motion artifacts to estimate the motion [6], [7]. We have previously described an iterative method to estimate and compensate for the head motion in clinical (helical) CT scans [8]. In the present study, we extend that approach to dental imaging applications. We will describe how the previous method has been adapted to overcome new challenges encountered in this application. The proposed method is evaluated with simulations, comparing motion-compensated reconstruction to reconstruction from motion-free data. In the following we define the full field view (FFOV) as the entire reconstructed region, ROI as the fully sampled region which is the same as the scan FOV, background as the region outside ROI and within the FFOV.

Manuscript received Apr. 30, 2017. This work was supported in part by the IWT MIRIAD SBO project and by the KU Leuven IMIR project.

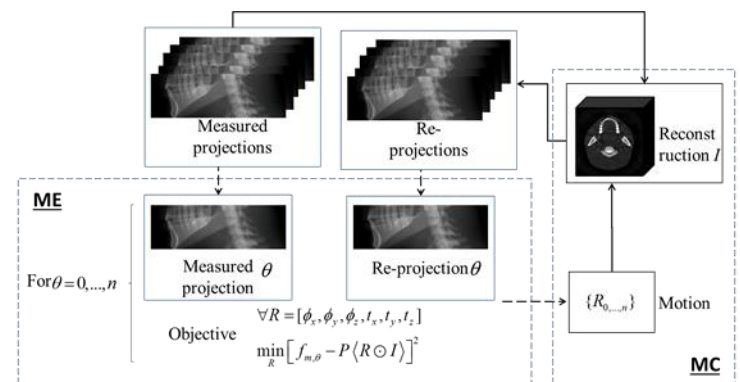
T. Sun and J. Nuyts are with the Medical Imaging Research Center, Department of Nuclear Medicine, KU Leuven, Belgium (tao.sun@uzleuven.be).

R. Fulton is with the Faculty of Health Sciences and School of Physics, University of Sydney, and the Department of Medical Physics, Westmead Hospital, Westmead, Australia.

## II. METHOD

### A. A revisit of the previous approach

Our previously described approach performs motion correction on clinical helical CT scans [8]. That method assumes that the rigid pose (motion) of the measured object may be different for each projection view. Consequently, a rigid transformation representing the object pose is estimated (Motion Estimation (ME) in Fig. 1) by a 3D-2D registration process for every view. A compensation for changes in pose during the scan is applied in reconstruction by incorporating the motion into the system matrix (Motion Compensation (MC) in Fig. 1). The motion-corrected image and the motion estimate are alternately updated to increase the likelihood, and the iterations are stopped when the estimated motion seems to have converged. This approach has been shown to effectively suppress the motion artifacts in helical CT scans with different setups and various scanners.



ME – Motion Estimation; MC – Motion Compensation.

$n$  is the total number of views,  $\theta$  is index of the projection view.

$I$  is the reconstructed image,  $R$  is the 6 degrees-of-freedom rigid motion,  $R \odot I$  is the transformed reconstructed image by  $R$ .

$P$  is the process of forward-projection at view  $\theta$ ,  $f_{m,\theta}$  is the measured projection at view  $\theta$ .

Fig. 1 General Motion Correction/Motion Compensation (ME/MC) scheme in [8]. One iteration of ME/MC involves 1 ME step and 1 MC step. The ME step attempts to adjust the object pose at each view to minimize the difference between the measured projections and the re-projected object. The MC step compensates for the motion during the scan in the iterative reconstruction process, by incorporating the motion estimates into the system matrix.

### B. New challenge in dental ROI imaging

Some important differences exist between helical CT and cone-beam CT, which may affect ME/MC on a dental scan. The most significant are the differences in axial and transaxial truncation. The circular scan with constant axial FOV in dental cone-beam CT is expected to facilitate ME/MC. On the other hand, dental cone-beam CT typically uses transaxial truncation to reduce the irradiated volume, which is expected to adversely affect ME/MC. Specifically, the ME step is based on re-projection, requiring a FFOV reconstructed image, which is not available in a ROI scan. In addition, the MC step uses an iterative reconstruction, which requires a FFOV reconstructed

image during forward/back-projection. Hence insufficient information outside the fully sampled ROI in a FFOV image will induce errors when using above ME/MC scheme. These errors could be streak artifacts in the reconstructed image after every iteration of MC, and inaccurate estimated motion after every iteration of ME

Another concern is that the information in the background, while not of clinical importance, but is required by an iterative reconstruction algorithm. An analytical reconstruction algorithm such as Feldkamp-Davis-Kress (FDK) can restrict the computations to the ROI, making it very efficient for such applications. In contrast, when an iterative reconstruction algorithm is used, the entire object must be reconstructed. Since our current motion compensation approach relies on iterative reconstruction, there is value in minimizing the amount of computations devoted to the background region, without compromising on reducing the motion artifacts.

### C. Improved Patch-based ME/MC

To address the above challenges, we implemented an improved Patch-based ME/MC. Patch-based reconstruction approaches have been proposed for various applications in CT imaging [9], [10]. The idea is that a reconstruction volume can be divided into interesting patches and not-so-important patches. For each of these patches different resolution model can be defined. Following [10], the patches were updated sequentially, each patch was considered as a group of pixels in a grouped coordinate algorithm. Sequentially updating groups of pixels is known to improve convergence, e.g. in the update equation of Maximum-Likelihood-Transmission-Reconstruction (MLTR) (Eq. 1), the denominator of the update steps will be smaller when the area of the updated patch is smaller:

$$\mu_j^{new} = \mu_j + \frac{a_j \sum_i c_{ij} (\bar{y}_i - y_i)}{\sum_i c_{ij} (\sum_k c_{ik} a_k) \bar{y}_i} \quad (1)$$

where

$$\begin{cases} a_j = 1 & \text{if } j \in \text{patch} \\ a_j = 0 & \text{if } j \notin \text{patch} \end{cases}$$

$i$  is the index of the projection lines,  $y_i$  is the measured transmission scan,  $\bar{y}_i$  is the estimated transmission scan, computed from the current reconstructed image  $\mu = \{\mu_j\}$ , with  $\mu_j$  is the linear attenuation coefficient in voxel  $j$ .  $c_{ij}$  is the intersection length of projection line  $i$  with voxel  $j$ . Motion correction can be done by adjusting the system matrix on-the-fly.

In this study, we propose to use such a patch-based reconstruction in ME/MC, to accelerate the iterative reconstructions. By applying this technique, we believe the two concerns in II. B can be mitigated. We defined two patches for dental ROI imaging (Fig. 2a):

high-res patch – the patch containing the teeth inside the fully sampled ROI where a smaller voxel size will be used.

low-res patch – the patch comprising the remainder of the FFOV where a coarser resolution model will be used.

Specifically, both ME and MC need to be adjusted for the patch-based implementation. For ME, the re-projection process involved the forward projections with different resolutions for different patches. For MC, update of the image can be divided into 2 steps (Fig. 2b) – a first update performed only in the high-res patch, and a sequential update performed in both the high-res patch and low-res patch:

#### 1) First update on high-res patch

We want the high-res patch to contain the high contrast structures, i.e. the teeth and the surrounding structures inside the fully sampled ROI, because they provide the most useful information for ME. Hence we first performed an initial FFOV FDK reconstruction, and then defined one high-res patch and one low-res patch by thresholding and dilating (Fig. 2a). During a reconstruction in MC (Fig. 1), the first update was limited to voxels within the high-res patch using MLTR. A L1-norm total variation (TV) regularization [11] was applied in the iterative reconstruction to enforce the high-frequency structures while reducing the streak artifacts surrounding the teeth in the high-res patch.

#### 2) Sequential update on both patches

Following the first update in the high-res patch, a sequential update was performed for both the low-res patch and high-res patch. The voxel size in the low-res patch is 4 times larger than the one in the high-res patch. MLTR performed alternate updates for two patches (where the high-res patch update is with TV).

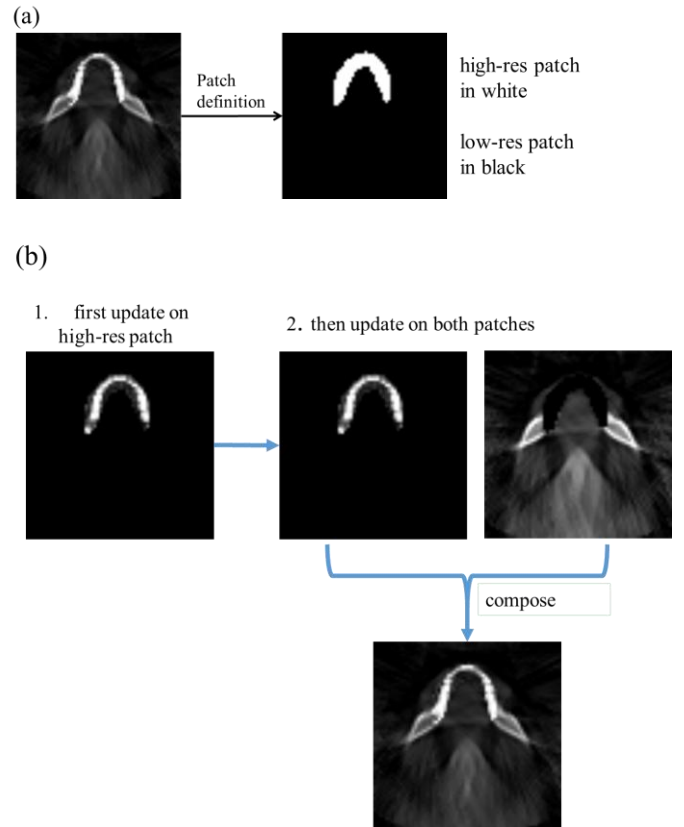


Fig. 2 (a) The patch definition for dental ROI imaging. (b) The patch-based improvement in a single iterative reconstruction process in MC. A first update was only performed in the high-res patch, and a sequential update was performed in the high-res and the low-res patches alternately.

#### D. Final reconstruction

On completion of the iterative ME/MC process, a final MLTR reconstruction was performed using the final estimated motion. To accelerate this reconstruction, the starting image was created from a FDK reconstruction with the estimated motion. For this purpose, an approximate circular FDK algorithm was implemented, where a first order motion compensation is obtained by taking the motion for each view into account in the back-projection step.

### III. EXPERIMENTS AND RESULTS

#### A. Phantom and motion

A digital phantom (Fig. 3) was used in all simulations. It was discretized into an image of  $256 \times 256 \times 70$  voxels with a voxel size of  $1.0 \times 1.0 \times 1.0$  mm<sup>3</sup>. A detector with  $200 \times 80$  detector pixels of  $1.0 \times 1.0$  mm<sup>2</sup> was simulated to create the transaxially truncated projections. The distance between the X-ray source and the detector was 575.0 mm, the distance between the detector and the rotation center was 216.5 mm. The scan FOV diameter was about 125.0 mm.

The head motion of a volunteer recorded over 5 second period (Fig. 4) was applied to the digital phantom while cone-beam projections were computed. The total simulate scan duration was 5 second. The total number of views was 360 covering 1 full rotation (360°). The projections were simulated with the same projector which was used during the reconstruction. Similar to helical CT, we assume that the motion within one cone-beam projection view is negligible. Hence there was no motion simulated within one projection view.

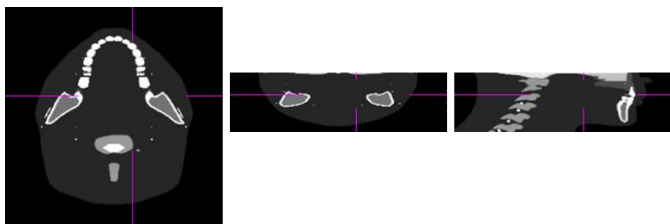


Fig. 3 The digital phantom that used in the simulations.

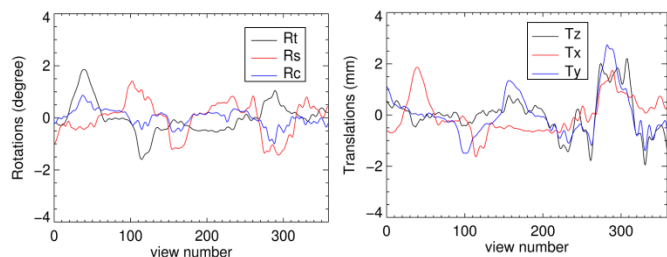


Fig. 4 The recorded motion segment to generate the motion-contaminated projections. The motion itself and details of how it was recorded can be found in [12].

#### B. Design of the experiments

From the simulated motion-contaminated projections, we computed the final reconstructed images from four different experiments: one with the compensation using the exact simulated motion, one without any compensation, one with ME/MC and one with Patch-based ME/MC. We aimed to compare the image quality and computation time in these cases. Details of how these final images in four experiments were obtained are listed below.

##### 1) Reference image

A reference image was obtained from an MLTR reconstruction with the exact simulated motion taken into account, starting from an initial-corrected FDK image. The iterative reconstruction parameters were: 4 iterations, 40 subsets, voxel size  $1.0 \times 1.0 \times 1.0$  mm<sup>3</sup>.

##### 2) Image w/o compensation

An MLTR reconstruction was performed, starting from an initial FDK reconstruction. No motion compensation was

applied. The iterative reconstruction parameters were the same as in the experiment to generate the reference image.

##### 3) Image with ME/MC

In one MC, the MLTR algorithm updated the FFOV image (4 reconstruction iterations 40 subsets, resolution  $1.0 \times 1.0 \times 1.0$  mm<sup>3</sup>). The total number of ME/MC iterations was 40 (1 iteration comprised 1 ME and 1 MC, as in Fig. 1). A final MLTR reconstruction was performed with the final estimated motion taken into account, starting from an initial-corrected FDK image.

##### 4) Image with Patch-based ME/MC

In one MC, the MLTR algorithm updated the high-res patch first with TV regularization (2 iterations 40 subsets, resolution  $1.0 \times 1.0 \times 1.0$  mm<sup>3</sup>), and then updated the two patches alternately (2 iterations 40 subsets, high-res patch resolution  $1.0 \times 1.0 \times 1.0$  mm<sup>3</sup> with TV, low-res patch resolution  $4.0 \times 4.0 \times 4.0$  mm<sup>3</sup> without regularization). In one ME, re-projection was done by combining the forward projections of the two patches. The total number of iterations of ME/MC was 40. A final MLTR reconstruction was performed with the final estimated motion taken into account, starting from an initial-corrected FDK image.

### C. Results

Fig. 5 shows the resulting images from the four experiments. Compared to the reference image, the image without any compensation was clearly contaminated by motion artifacts (red arrow) and not suitable for diagnostic purposes. After applying ME/MC to the measured data, most of the artifacts were suppressed (after 15 iterations of ME/MC, the improvement on motion estimation stopped). But there was still some resolution loss. The Patch-based ME/MC reduced this resolution loss and did so at a lower computation time with the same number of iterations. The Patch-based ME/MC continued to improve the image even after the original approach failed to improve further. This is confirmed in the quantitative plots in Fig. 6 and Fig. 7.

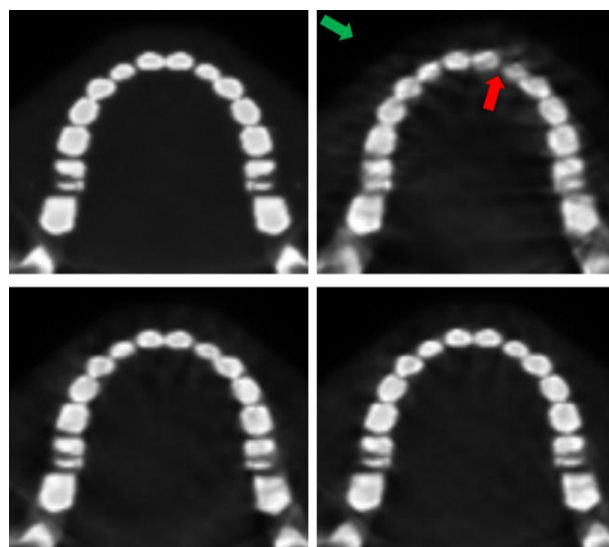


Fig. 5 The final reconstructed images in the four experiments. The top-left image is reference image from a reconstruction with the exact motion (II.B.1); The top-right image is without any compensation (II.B.2); the bottom-left image is with ME/MC (II.B.3, 15 iterations); the bottom-right image is with Patch-based ME/MC (II.B.4, 15 iterations).

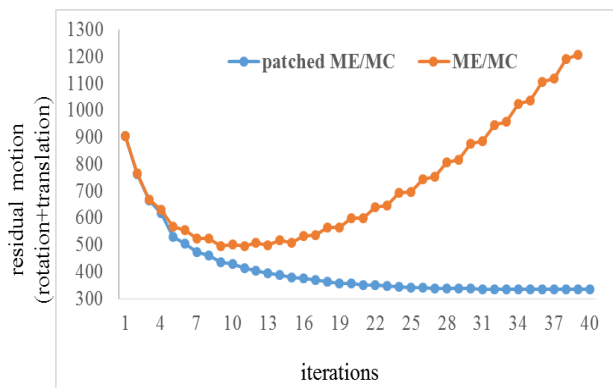


Fig. 6 Evaluation of the estimated motion by ME/MC and Patch-based ME/MC at every iteration, using residual motion errors (squared difference between the estimated motion and true motion - rotations in degrees, translations in mm). With 40 iterations, the total time of ME/MC was 2h13m, the time of the Patch-based ME/MC was 1h30m.

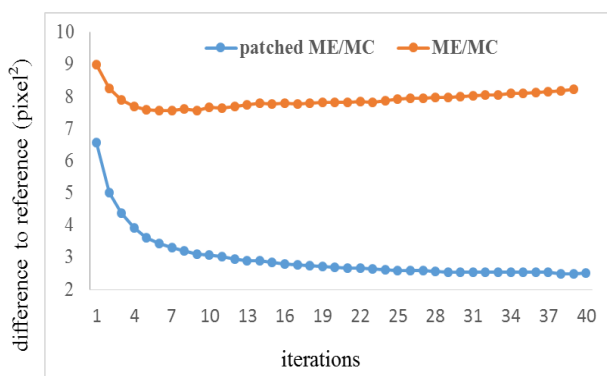


Fig. 7 A comparison between ME/MC and with Patch-based ME/MC images at each iteration, using relative image differences (squared difference between compensated reconstruction and reference image) in the ROI.

#### IV. DISCUSSION AND CONCLUSION

In this paper, we proposed a motion estimation and compensation approach for dental cone-beam CT imaging with transaxial truncation, the implementation of which only requires the measured raw data. Since no additional measurements are needed, it can be applied retrospectively to any dental scan data.

The proposed approach works reasonably well despite the severe artifacts outside the high-res patch, where the reconstruction is handicapped by a limited angle problem. It has been previously shown that the high-res patch can in principle be reconstructed exactly if it contains a portion of air background (intensity known as zero) [13], which is often the case in dental imaging (green arrow in Fig. 5). Moreover, even in the background, spatial frequencies are better reconstructed if they contribute more information to the measured projections (typically edges which are parallel to the projection lines). This implies that the reconstructed low-res patch still contains the relevant edges needed to align measured and forward projected views, which is the essence of the original ME/MC scheme.

The estimated motion is not always identical to the true simulated motion. One reason, as described previously, is that the background cannot be reconstructed exactly, which may propagate the errors of non-exact reconstruction into ME. However, our aim is to compensate for motion artifacts rather than to estimate the motion itself.

Unlike a clinical (helical) CT scan, a normal dental scan has a small number of views (300~700) acquired in a full or half rotation. Hence the computation requirement to apply the compensation in dental imaging is less demanding. Currently, the entire Patch-based ME/MC process takes ~90 minutes (40

ME/MC iterations) for the moderate motion shown in Fig. 3. This indicates that more time would be needed to process a real scan where a smaller voxel size is often used. On the other hand, by introducing proper acceleration techniques, the processing time can be significantly reduced.

In this preliminary study, we only showed results from simulations. Further testing on real clinical data is ongoing. The effect of factors such as the size of the FOV, the use of an offset scan, number of views, half or full rotation scan and presence of dental implants on the performance of the proposed approach will be assessed.

#### V. ACKNOWLEDGEMENT

The authors want to thank Dr. Koen Michielsen and Prof. Reinilde Jacobs for providing the digital phantom.

#### REFERENCES

- [1] K. Donaldson, S. O'Connor, and N. Heath, "Dental cone beam CT image quality possibly reduced by patient movement," *Dentomaxillofacial Radiol.*, vol. 42, no. 2, pp. 3–4, 2013.
- [2] R. Spin-Neto, J. Mudrak, L. H. Matzen, J. Christensen, E. Gottfredsen, and A. Wenzel, "Cone beam CT image artefacts related to head motion simulated by a robot skull: Visual characteristics and impact on image quality," *Dentomaxillofacial Radiol.*, vol. 42, no. 2, 2013.
- [3] C. Nardi, C. Borri, F. Regini, L. Calistri, A. Castellani, C. Lorini, and S. Colagrande, "Metal and motion artifacts by cone beam computed tomography in dental and maxillofacial study," *Radiol. Medica*, vol. 120, no. 7, pp. 618–626, 2015.
- [4] C. J. Ritchie, C. R. Crawford, J. D. Godwin, K. F. King, and Y. Kim, "Correction of Computed Tomography Motion Artifacts Using Pixel-Specific Back-Projection," *IEEE Trans. Med. Imaging*, vol. 15, no. 3, pp. 333–342, 1996.
- [5] W. Lu and T. R. Mackie, "Tomographic motion detection and correction directly in sinogram space," *Phys. Med. Biol.*, vol. 47, no. 8, pp. 1267–1284, Apr. 2002.
- [6] Y. Kyriakou, R. M. Lapp, L. Hillebrand, D. Ertel, and W. a Kalender, "Simultaneous misalignment correction for approximate circular cone-beam computed tomography," *Phys. Med. Biol.*, vol. 53, no. 22, pp. 6267–6289, Nov. 2008.
- [7] A. Kingston, A. Sakellariou, T. Varslot, G. Myers, and A. Sheppard, "Reliable automatic alignment of tomographic projection data by passive auto-focus," *Med. Phys.*, vol. 38, no. 9, pp. 4934–4945, Sep. 2011.
- [8] T. Sun, J.-H. Kim, R. Fulton, and J. Nuyts, "An iterative projection-based motion estimation and compensation scheme for head X-ray CT," *Med. Phys.*, vol. 43, no. 10, pp. 5705–5716, 2016.
- [9] L. Yu, Y. Zou, E. Y. Sidky, C. A. Pelizzari, P. Munro, and X. Pan, "Region of interest reconstruction from truncated data in circular cone-beam CT," *IEEE Trans. Med. Imaging*, vol. 25, no. 7, pp. 869–881, 2006.
- [10] K. Van Slambrouck and J. Nuyts, "Metal artifact reduction in computed tomography using local models in an image block-iterative scheme," *Med. Phys.*, vol. 39, no. 11, pp. 7080–93, Nov. 2012.
- [11] E. Y. Sidky and X. Pan, "Image reconstruction in circular cone-beam computed tomography by constrained, total-variation minimization," *Phys. Med. Biol.*, vol. 53, no. 17, pp. 4777–4807, 2008.
- [12] J.-H. Kim, J. Nuyts, A. Kyme, Z. Kuncic, and R. Fulton, "A rigid motion correction method for helical computed tomography (CT)," *Phys. Med. Biol.*, vol. 60, no. 5, pp. 2047–73, Mar. 2015.
- [13] M. Defrise, F. Noo, R. Clackdoyle, and H. Kudo, "Truncated Hilbert transform and image reconstruction from limited tomographic data," *Inverse Probl.*, vol. 22, no. 3, pp. 1037–1053, Jun. 2006.